

Band edge evolution of transparent $\text{ZnM}_2^{\text{III}}\text{O}_4$ ($M^{\text{III}} = \text{Co, Rh, Ir}$) spinels

Matthew J. Wahila,¹ Zachary W. Lebens-Higgins,¹ Adam J. Jackson,^{2,3} David O. Scanlon,^{2,3} Tien-Lin Lee,⁴ Jiaye Zhang,⁵ Kelvin H. L. Zhang,^{5,6,*} and Louis F. J. Piper^{1,7,†}

¹*Department of Physics, Applied Physics and Astronomy, Binghamton University, Binghamton, New York 13902, USA*

²*Department of Chemistry, University College London, London WC1H 0AJ, United Kingdom*

³*Thomas Young Centre, University College London, London WC1E 6BT, United Kingdom*

⁴*Diamond Light Source Limited, Harwell Science and Innovation Campus, Didcot OX11 0DE, United Kingdom*

⁵*State Key Laboratory of Physical Chemistry of Solid Surfaces, College of Chemistry and Chemical Engineering, Xiamen University, Xiamen 361005, China*

⁶*Department of Materials Science & Metallurgy, University of Cambridge, Cambridge CB3 0FS, United Kingdom*

⁷*Material Science & Engineering, Binghamton University, Binghamton, New York 13902, USA*



(Received 1 April 2019; revised manuscript received 2 August 2019; published 15 August 2019)

$\text{ZnM}_2^{\text{III}}\text{O}_4$ ($M^{\text{III}} = \text{Co, Rh, Ir}$) spinels have been recently identified as promising p -type semiconductors for transparent electronics. However, discrepancies exist in the literature regarding their fundamental optoelectronic properties. In this paper, the electronic structures of these spinels are directly investigated using soft/hard x-ray photoelectron and x-ray absorption spectroscopies in conjunction with density functional theory calculations. In contrast to previous results, ZnCo_2O_4 is found to have a small electronic band gap with forbidden optical transitions between the true band edges, allowing for both bipolar doping and high optical transparency. Furthermore, increased d - d splitting combined with a concomitant lowering of Zn s/p conduction states is found to result in a ZnCo_2O_4 (ZCO) < ZnRh_2O_4 (ZRO) \approx ZnIr_2O_4 (ZIO) band gap trend, finally resolving long-standing discrepancies in the literature.

DOI: [10.1103/PhysRevB.100.085126](https://doi.org/10.1103/PhysRevB.100.085126)

I. INTRODUCTION

Transparent oxide semiconductors (TOSs) combining tunable electrical conductivity and optical transparency hold great promise for a wide range of applications, including solar cells, flat-panel displays, UV photodetectors, and transparent transistors [1–4]. Most TOSs to date are n -type semiconductors composed of post-transition-metal oxides, e.g., In_2O_3 , Ga_2O_3 , SnO_2 , and ZnO , as their metal ns -derived conduction states give rise to dispersive conduction band minima with a low electron effective mass. In contrast, p -type conduction in these oxides is typically poor due to their localized O $2p$ -derived valence band maxima. However, hybridization between the O $2p$ and metal orbitals has been shown to improve hole dispersion, as in some Cu^+ -based delafossites, Cr^{3+} -based oxides, and post-transition-metal oxides with a filled lone pair state (ns^2) [5–10]. Unfortunately, some common theoretical methods are known to be unreliable when predicting the properties of mixed oxides with potentially complex local interactions [11], hampering computation-led materials genome initiatives that exist to accelerate the discovery of these materials.

Herein we illustrate the benefits of using careful experimental studies to guide computational efforts by explaining the optoelectronic properties of $\text{ZnM}_2^{\text{III}}\text{O}_4$ ($M^{\text{III}} = \text{Co, Rh, Ir}$) spinels, which have been identified as promising p -type TOSs by recent studies [12–15]. Some studies have even indicated

that transparent ZnCo_2O_4 may be well suited for complementary metal-oxide-semiconductor (CMOS) electronics applications [16], as it is amenable to bipolar doping with both n or p type possible through control of the oxygen content [17]. This bipolar dopability indicates that ZnCo_2O_4 , and likely ZnRh_2O_4 and ZnIr_2O_4 as well, must possess small electronic band gaps despite their high optical transparency (i.e., wide optical band gaps) [18–21]. In addition, it has been shown that the local O-Rh-O octahedral network in ZnRh_2O_4 can be preserved in an amorphous phase, allowing for good hole conduction pathways without high film crystallinity [22,23]. This is in stark contrast to other p -type TOSs, such as CuAlO_2 delafossite, where disorder disrupts the linear O-Cu-O coordination and greatly impedes hole conduction [5].

In spite of their potential promise, many discrepancies exist in the literature regarding the fundamental properties of these $\text{ZnM}_2^{\text{III}}\text{O}_4$ spinels. There is a clear lack of consensus regarding band gap magnitudes, with some studies suggesting a decrease in the band gap from Co to Rh and others an increase from Co to Rh [13,17,24,25]. Optical studies have reported band gaps of 2.63–2.8 eV for ZnCo_2O_4 [17,26], a much smaller 2 eV optical gap for ZnRh_2O_4 [13,27], and a range of values between 2.1 and 2.7 eV for ZnIr_2O_4 [14]. Meanwhile, a more wide-ranging study by Dekkers *et al.* reports drastically different values of 2.26, 2.74, and 2.97 eV for ZnCo_2O_4 , ZnRh_2O_4 , and ZnIr_2O_4 , respectively [28].

Theoretical studies have attempted to resolve these conflicting results with mixed success. As many common density functional theory (DFT) methods are known to underestimate the band gaps of metal oxides, some have attempted to

*kelvinzhanghl@gmail.com

†lpiper@binghamton.edu

improve accuracy through the use of more complex hybrid functionals [25,29,30]. However, others have questioned the accuracy of these methods regarding mixed cation oxides, reporting that calculations using the Perdew-Burke-Ernzerhof (PBE0) hybrid functional resulted in the Co *d-d* splitting of Co-doped ZnO being overestimated by as much as 300% compared to experiment [11]. It is clear that a thorough experimental study is needed to understand these spinels and resolve the discrepancies in the literature.

In this paper, a set of high-quality ZnCo_2O_4 (ZCO), ZnRh_2O_4 (ZRO), and ZnIr_2O_4 (ZIO) epitaxial thin films are investigated using synchrotron-based x-ray spectroscopy techniques to discern the true band edge structures. These results are then combined with DFT PBEsol calculations [31–37] to confirm orbital compositions of the band edges and explain the observed optoelectronic trends. The results reveal that these $\text{ZnM}_2^{III}\text{O}_4$ spinels possess smaller electronic gaps than previously measured by optical techniques, explaining their bipolar doping potential. In addition, overlap of the Zn *s* and M^{III} *d* orbitals in ZnIr_2O_4 due to shrinking O 2*p*-Zn 4*s/p* splitting is responsible for the confusion in the literature surrounding the band gap evolution.

II. EXPERIMENTAL METHODS

$\text{ZnM}_2^{III}\text{O}_4$ ($M^{III} = \text{Co, Rh, Ir}$) thin films possessing the spinel structure, shown in Fig. 1(a), were fabricated via pulsed laser deposition using a 248-nm KrF excimer laser with an energy density of 1.0 J cm^{-2} and a repetition rate of 5 Hz. The substrate temperature for all films was kept at 475°C with an oxygen partial pressure of 150 mTorr for ZCO/ZRO, and 30 mTorr for ZIO. Higher oxygen partial pressures were found to give higher conductivities, while both lower and higher substrate temperatures of 375 and 550°C were found to lead to the growth of a ZnO second phase. The ZCO films were grown epitaxially on $5 \times 5\text{ mm MgAl}_2\text{O}_4(001)$ substrates, while ZRO and ZIO films were grown epitaxially on $\text{MgO}(001)$, as it is difficult to grow these films on MgAl_2O_4 due to a large lattice mismatch.

Shown in Figs. 1(b)–1(d), these growth parameters resulted in crystalline, epitaxial thin films around 25 nm in thickness, as confirmed by reflection high-energy electron diffraction (RHEED), x-ray diffraction (XRD), and reciprocal space mapping (RSM). Our epitaxial ZCO is found to have in-plane and out-of-plane lattice dimensions of 8.08 and 8.23 Å, respectively, compared to 8.108 Å expected for bulk from the literature. Our epitaxial ZRO has in-plane and out-of-plane lattice dimensions of 8.424 and 8.730 Å, respectively, compared to 8.510 Å expected for bulk from the literature. And our epitaxial ZIO has in-plane and out-of-plane lattice dimensions of 8.445 and 8.709 Å, respectively.

Ultraviolet-visible (UV-vis) transmittance spectra were measured on the films and substrate references. Optical absorption coefficients were then calculated from the spectra after subtracting out any contributions from the substrates using the thin film approximation $T \approx (1 - R)^2 e^{-\alpha d}$, where *T* is the transmittance, *R* is the reflectance, and *d* is the film thickness.

Hard x-ray photoelectron spectroscopy (HAXPES) measurements were performed with a $\sim 6\text{ keV}$ photon energy at

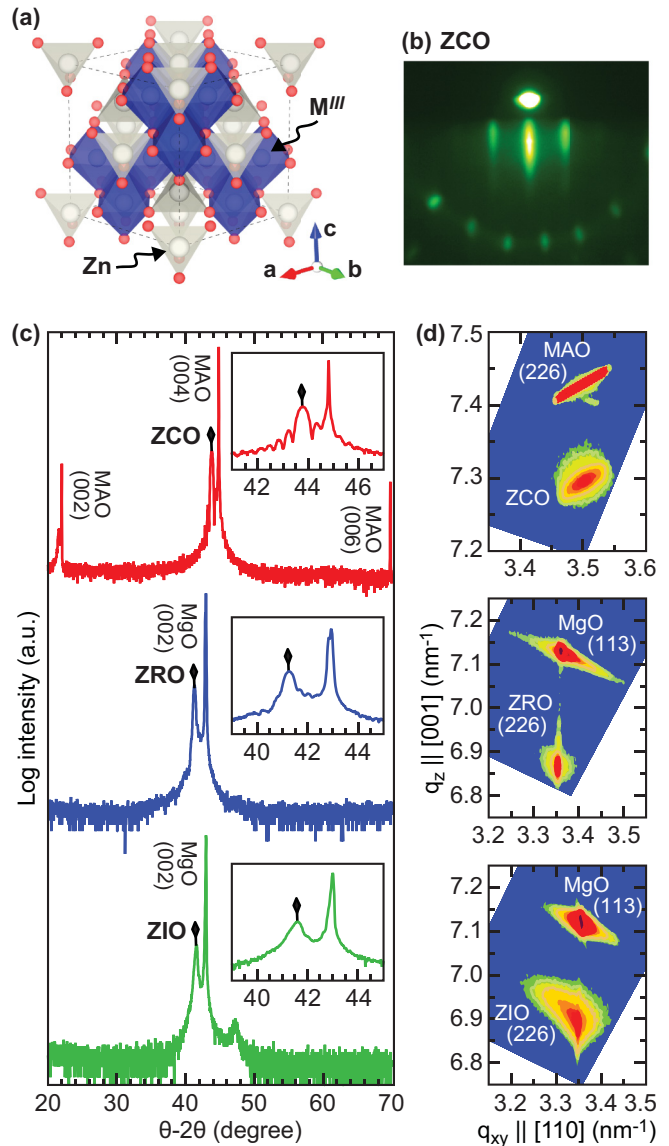


FIG. 1. (a) The spinel structure of $\text{ZnM}_2^{III}\text{O}_4$, where the M^{III} cations (Co, Rh, or Ir) occupy octahedral sites (blue) and Zn occupy tetrahedral sites (gray). (b) Reflection high-energy electron diffraction (RHEED) image taken on a ZCO film. (c) Out-of-plane θ - 2θ x-ray diffraction (XRD) for the ZCO, ZRO, and ZIO films. (d) Reciprocal space maps (RSM) for ZCO around the substrate MgAl_2O_4 (MAO) (226) reflection and for ZRO/ZIO around the substrate $\text{MgO}(113)$ reflection.

the I09 beamline of the Diamond Light Source (DLS) in Oxfordshire, U.K. HAXPES spectra were energy resolved and measured using a VG Scienta EW4000 high-energy electron-energy analyzer with a 56° acceptance angle. The HAXPES photon beam was monochromated using a Si(111) double-crystal monochromator followed by a Si(004) channel-cut high resolution monochromator, resulting in an overall energy resolution of $< 50\text{ meV}$ [38–40].

X-ray absorption spectroscopy (XAS) was performed at beamline I09, and also at beamlines 6 and 8 of the Advanced Light Source in Berkeley, CA. All XAS spectra were taken in total electron yield (TEY) mode, with an effective resolution

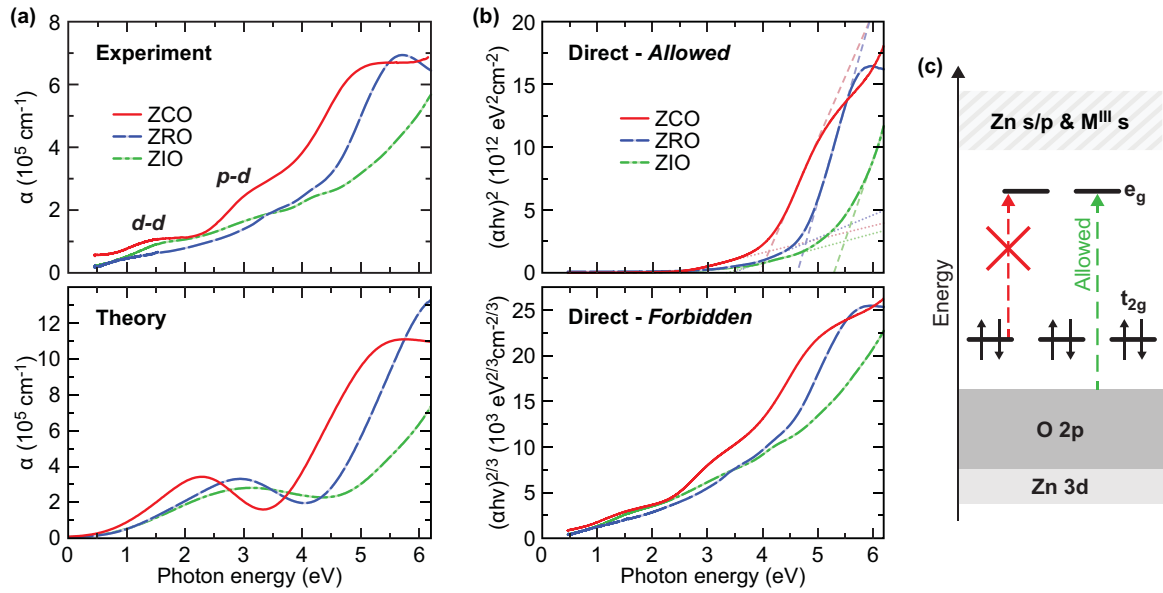


FIG. 2. (a) Optical absorption coefficients of ZCO, ZRO, and ZIO derived from (top) optical transmittance/reflectance measurements and (bottom) atomistic calculations. (b) Tauc plots emphasizing (top) direct allowed transitions and (bottom) direct forbidden transitions. Fit lines for the main optical absorption edge (dashed lines) and weaker p - d associated transitions (dotted lines) are given. (c) Proposed schematic of the near E_F band configuration for $\text{ZnM}_2^{\text{III}}\text{O}_4$ spinels.

of ~ 200 meV. The absorption spectra were normalized to the current from either a reference Au-coated mesh in the path of the incident photon beam or the last mirror before the sample. Energy calibration was performed using the first- and second-order diffraction Ti $L_{3,2}$ -edge and O K -edge absorption features of a rutile TiO_2 reference.

Density functional theory (DFT) calculations were performed using the Vienna *ab initio* simulation package (VASP) [31] with a projector augmented-wave pseudopotential [32,33]. A 500-eV cutoff plane-wave basis set was employed for electronic structure calculations using the PBEsol exchange-correlation functional [34]. The initial cubic structure for ZnCo_2O_4 ($Fd\bar{3}m$ space group) was drawn from the Materials Project database [35,36]. After convergence testing of the Brillouin-zone sampling for ZnCo_2O_4 , a $4 \times 4 \times 4$ Γ -centered \mathbf{k} -point mesh was used to optimize the lattice parameters and atomic positions of ZnCo_2O_4 and derived cells of ZnRh_2O_4 and ZnIr_2O_4 , reducing forces to less than 10^{-3} eV/Å. Force/energy evaluations used an energy convergence criterion of 10^{-6} eV with 0.1 eV Gaussian broadening.

Density of states (DOS) calculations were performed using the optimized structures with stricter energy convergence (10^{-7} eV between final steps), denser Brillouin-zone sampling ($6 \times 6 \times 6$ Γ -centered mesh), and increased Gaussian broadening (0.2 eV). Band structures were calculated non-self-consistently using the charge density data computed during DOS calculations. Optical absorption coefficients were computed at the same geometry using a $14 \times 14 \times 14$ \mathbf{k} -point mesh and integrating with the Blöchl-corrected tetrahedron method [37]. The frequency-dependent dielectric matrix was computed within VASP by summation over empty states, obtaining the real part by a Kramers-Kronig transformation. This was then converted to absorption via the extinction coefficient.

III. RESULTS AND DISCUSSION

Figure 2(a) shows the photon energy-dependent absorption coefficients derived from ultraviolet-visible (UV-vis) transmittance spectra, as well as predicted from theoretical calculations. Qualitatively, the general shapes of the measured and predicted absorption edges agree quite well. Shown in Fig. 2(b), band gaps can be quantitatively determined from absorption spectra using Tauc analysis, where $(\alpha h\nu)^{1/r}$ is plotted versus $h\nu$ using an r value corresponding to the type of optical transition occurring between the band edges [41,42]. After fitting a line to the predominantly linear region of this Tauc plot, the x intercept of said line provides an approximate value for the onset of optical absorption (i.e., the band gap), provided there is negligible background signal at photon energies below the absorption onset.

Assuming that the band gap is direct and that optical transitions are allowed ($r = 1/2$), as in the top of Fig. 2(b), the strongest absorption onsets (dashed lines) are found to occur around 4.1, 4.7, and 5.5 eV for ZCO, ZRO, and ZIO, respectively, when taking into account the background from the weaker absorptions at lower energies. These values are all far too large to correspond to band gaps previously reported in the literature [28]. Fitting a line to the weaker optical absorptions (dotted lines) provides a slightly different band gap order of $\text{ZCO} < \text{ZRO} \simeq \text{ZIO}$, with energetic onsets of 2.5, 3.5, and 3.3 eV for ZCO, ZRO, and ZIO, respectively. These values are much closer in magnitude to some previously reported values for the optical band gaps [17,26,28]. However, a Tauc plot where $r = 1/2$ is likely not the best method for investigating the band gaps of these spinels, as optical transitions between the band edges would be forbidden if the band edges are truly $M^{\text{III}} d$ orbital in origin as expected.

Due to the octahedral ligand coordination of the M^{III} cation in the spinel structure, the $M^{III} nd^6$ orbitals will split into three t_{2g} and two e_g states, as depicted in Fig. 2(c). In this configuration, the lower-energy (t_{2g}) states will be completely filled while the higher (e_g) states will be completely empty [28,43]. This $d-d$ splitting is typically on the order of $\sim 2 - 3$ eV for metal oxides with octahedral coordination [11,43,44], while the O $2p$ -Zn $4s/p$ splitting is typically larger, at ~ 3.4 eV for ZnO [11]. As such, it is highly likely that $M^{III} d$ -orbital states compose one if not both of the band edges in these spinels.

As ligand field ($d-d$) splitting typically increases with atomic number, it is not unreasonable to expect the band gaps of these spinels to increase in magnitude from Co to Rh to Ir [13]. While some previous experimental studies do not support this conclusion, these investigations are complicated by the fact that optical transitions between t_{2g} and e_g states do not represent a change in parity and are thus forbidden according to the Laporte rule. This makes the $d-d$ splitting in these spinels difficult to investigate using optical techniques alone, as the optical absorption due to transitions between the band edges should be incredibly weak [23,45].

Treating these spinels as direct band gap materials but with *forbidden* band edge transitions ($r = 3/2$), as in the bottom of Fig. 2(b), reveals a multitude of weak yet distinct absorption onsets extending down to 2 eV or below. In this case, the background at low energies is clearly non-negligible and must be properly accounted for in order to determine the band gaps with any accuracy [46]. Unfortunately, it is a nontrivial and rather subjective process to disentangle the true band edge absorption from all of the various effects potentially contributing to the background, such as wavelength-dependent reflections, scattering processes not accounted for by the reference standard, or absorption from ion vacancies or other defects. However, even without the determination of accurate numerical values for the band gaps, this analysis clearly indicates that although the majority of the optical absorption occurs above ~ 3 eV, the electronic band gaps of these spinels must be smaller.

Figure 3 shows the valence and conduction band spectra for ZCO, ZRO, and ZIO as measured by multiple x-ray spectroscopy techniques, as well as calculated using DFT. It must be noted that the ZRO appears to have some ZnO-like spectral contamination potentially caused by a zinc-rich surface layer or segregated crystallites, resulting in an over-representation of Zn-related states in the experimental spectra.

Combining both high-resolution hard x-ray photoelectron spectroscopy (HAXPES) [38–40] and x-ray absorption spectroscopy (XAS) provides crucial insight into the true evolution of both band edge. In ZCO, the sharp Co $3d$ t_{2g} and e_g peaks are found to make up the band edges, with a small $d-d$ splitting. In ZRO, the Rh $4d$ t_{2g} and e_g peaks show greater $d-d$ splitting than the Co $3d$, and they also appear significantly broadened in comparison. And in ZIO, the $d-d$ peak splitting appears by far the largest, however, additional features/shoulders are present on both band edges that cannot be assigned a pure Ir $5d$ character. These band edge changes result in an electronic band gap order of ZCO < ZRO \approx ZIO despite the apparently larger $d-d$ splitting of ZIO relative to ZRO, in agreement with some theoretical studies [25].

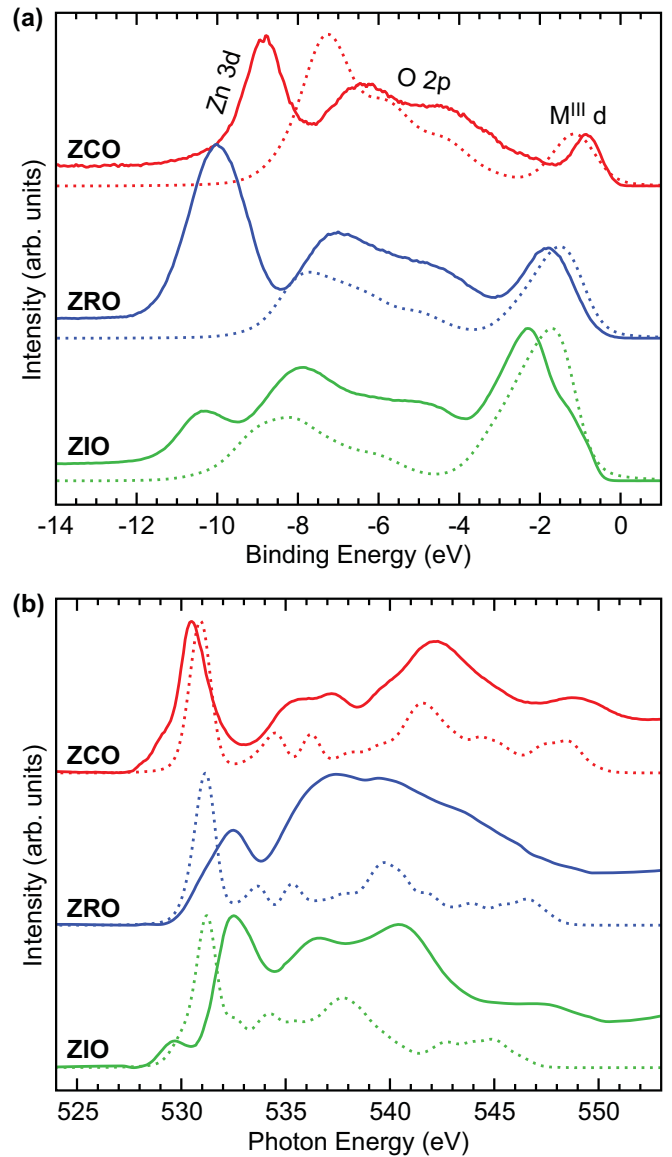


FIG. 3. (a) HAXPES (solid) and DFT PBEsol total density of states (dotted) of the ZCO, ZRO, and ZIO valence band region. (b) XAS oxygen K edge (solid) and DFT PBEsol oxygen $2p$ partial density of states (dotted) of the ZCO, ZRO, and ZIO conduction band region.

While several theoretical studies reported in the literature have attempted to simulate the electronic structures of these ZnM_2O_4 spinels [25,26,29,30], a large discrepancy exists regarding the magnitudes of predicted band gaps. In general, DFT calculations result in small band gaps (e.g., 0.57, 0.80, and 0.48 eV for $ZnCo_2O_4$ [25], $ZnRh_2O_4$, and $ZnIr_2O_4$, respectively), while the hybrid exchange-correlation functional of Heyd-Scuseria-Ernzerhof (HSE06) [25] and GW calculations [30] yield significantly large band gap values (e.g., 3.86, 2.87, and 2.47 eV for $ZnCo_2O_4$, $ZnRh_2O_4$, and $ZnIr_2O_4$, respectively). In this study, a comparison of our theoretical results with both the optical absorption spectra in Fig. 2 and the experimental density of states in Fig. 3 suggests that our

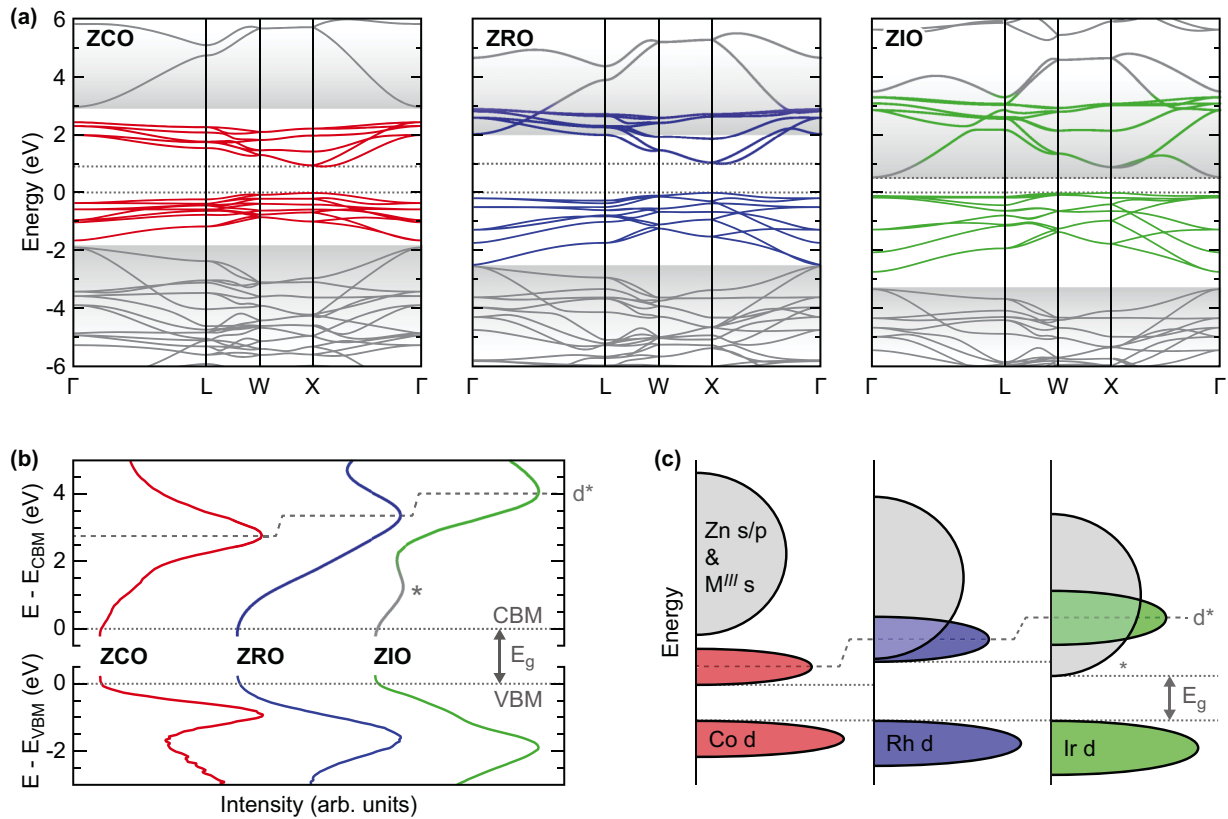


FIG. 4. (a) DFT calculated band diagrams for ZCO, ZRO, and ZIO. The $d-d$ split states (colored lines) and s/p -derived states (shaded background) are denoted. (b) Experimentally measured band edges of ZCO, ZRO, and ZIO. (c) Diagram of the proposed band edge evolution from ZCO to ZRO to ZIO. Additional states extending below the main Ir 5 d -derived conduction band states are denoted (*).

DFT PBEsol calculations can be used to provide valuable insight into the band edge evolution.

Although the DFT shown in Fig. 3 underestimates the energetic position of the Zn 3 d semicore level and the band gap magnitudes, which are both well-documented issues with some forms of DFT [11,21,47], the rest of the observed spectral features are fairly well reproduced. The calculated spectra show a clear increase in the $d-d$ splitting from ZCO to ZRO to ZIO despite the incorrect overall magnitude, in agreement with the experimental spectra and with previous studies [25,28,30]. The calculated spectra also reproduce the Rh 4 d broadening, as well as the additional features/shoulders on the Ir 5 d peaks, which are a result of a greater overlap and hybridization between the unoccupied $M^{III} e_g$ and the Zn s/p and $M^{III} s$ -orbital conduction states.

Figure 4 summarizes the band edge evolution of the $ZnM_2^{III}O_4$ series as observed in this study. Figure 4(a) displays the full DFT calculated band diagrams for the series, clearly showing the expected interaction between the different bands. Figure 4(b) then shows the experimentally observed band edges, which agree well with the predicted band edge evolution. While the band edges of $ZnCo_2O_4$ are both composed of sharp Co 3 d states fairly well separated from the Zn s/p -, O 2 p -, and Co s -related states, the band edges in $ZnRh_2O_4$ and $ZnIr_2O_4$ show far more interaction and overlap. This results in the observed $ZCO < ZRO \approx ZIO$ band gap trend and increasing band edge dispersion, which readily explains the better

p -type conduction in ZRO and ZIO. This is in agreement with a previous theoretical study which suggested the conduction band minimum (CBM) of ZIO might be composed of mixed Ir s and Zn s states due to a lowering of these conduction states below the Ir 5 d [25].

A simplified diagram of the observed band edge evolution is given in Fig. 4(c). While the $d-d$ splitting is found to progressively increase from Co to Ir, the Zn $s-p$ and $M^{III} s$ conduction band states simultaneously lower in energy. This results in a conduction band edge of mainly $M^{III} d$ character in ZCO, mixed $M^{III} d$, $M^{III} s$, and Zn s/p character in ZRO, and mainly $M^{III} s$ and Zn s/p character in ZIO. This model resolves the conflicting results of previous studies by allowing for both the $d-d$ splitting to increase with increasing atomic number as expected, and the electronic band gaps to progress in the order $ZCO < ZRO \approx ZIO$.

IV. CONCLUSIONS

These findings explain the observation of both n - and p -type conduction in $ZnCo_2O_4$ [17]. A small electronic band gap with forbidden optical transitions between the true band edges allows for both the observed doping capabilities and the high optical transparency, similar to some other transparent metal oxides such as crystalline SnO or $CuInO_2$ [8,48,49]. Furthermore, the increased conductivity of crystalline $ZnRh_2O_4$ and $ZnIr_2O_4$ relative to $ZnCo_2O_4$ [30] is explained by the

observed increase in hybridization at the band edges for these M^{III} cations. This conduction band edge hybridization suggests that n -type doping may also be possible in ZIO or even ZRO despite the slightly larger band gaps, provided their electron affinities remain large enough.

These results highlight the need for experimental confirmation of predicted electronic structures, especially when considering transparent mixed oxide systems such as these $ZnM_2^{III}O_4$ spinels. While certain methodologies may correctly predict the M^{III} d - d splitting or the O $2p$ and Zn s/p splitting, correctly reproducing all vital aspects of the spectra would likely require far more involved calculations with explicit on-site corrections for each cation [47]. And such corrections must still be informed by prior experimental results to have any real meaning, leading to a necessity for thorough experimental studies on these mixed oxide systems.

ACKNOWLEDGMENTS

K.H.L.Z. is grateful for funding support from the Herchel Smith Fellowship by University of Cambridge and the Thousand Youth Talents Program of China. We thank Diamond Light Source for access to beamline I09 (SI 16005), which contributed to the results presented here. We also thank beamline scientist Christoph Schlueter at Diamond Light Source for their assistance. This material is based upon work supported by the Air Force Office of Scientific Research under Award No. FA9550-18-1-0024. This work made use of the UCL Grace and Legion high-performance computing resources and the ARCHER U.K. National Supercomputing Service, via membership of the U.K.'s HEC Materials Chemistry Consortium, which is funded by the EPSRC (EP/L000202). A.J.J. and D.O.S. acknowledge support from the EPSRC (EP/N01572X/1).

-
- [1] T. Kamiya and H. Hosono, *NPG Asia Mater.* **2**, 15 (2010).
- [2] E. Fortunato, P. Barquinha, and R. Martins, *Adv. Mater.* **24**, 2945 (2012).
- [3] X. Yu, T. J. Marks, and A. Facchetti, *Nat. Mater.* **15**, 383 (2016).
- [4] H. Hosono, *Jpn. J. Appl. Phys.* **52**, 090001 (2013).
- [5] H. Kawazoe, M. Yasukawa, H. Hyodo, M. Kurita, H. Yanagi, and H. Hosono, *Nature (London)* **389**, 939 (1997).
- [6] H. Yanagi, S.-i. Inoue, K. Ueda, H. Kawazoe, H. Hosono, and N. Hamada, *J. Appl. Phys.* **88**, 4159 (2000).
- [7] Y. Ogo, H. Hiramatsu, K. Nomura, H. Yanagi, T. Kamiya, M. Kimura, M. Hirano, and H. Hosono, *Phys. Status Solidi A* **206**, 2187 (2009).
- [8] M. J. Wahila, K. T. Butler, Z. W. Lebens-Higgins, C. H. Hendon, A. S. Nandur, R. E. Treharne, N. F. Quackenbush, S. Sallis, K. Mason, H. Paik *et al.*, *Chem. Mater.* **28**, 4706 (2016).
- [9] K. H. L. Zhang, Y. Du, A. Papadogianni, O. Bierwagen, S. Sallis, L. F. J. Piper, M. E. Bowden, V. Shutthanandan, P. V. Sushko, and S. A. Chambers, *Adv. Mater.* **27**, 5191 (2015).
- [10] J. Y. Zhang, W. W. Li, R. L. Z. Hoyer, J. L. MacManus-Driscoll, M. Budde, O. Bierwagen, L. Wang, Y. Du, M. J. Wahila, L. F. J. Piper *et al.*, *J. Mater. Chem. C* **6**, 2275 (2018).
- [11] A. Walsh, J. L. F. Da Silva, and S.-H. Wei, *Phys. Rev. Lett.* **100**, 256401 (2008).
- [12] F.-L. Schein, M. Winter, T. Böntgen, H. Von Wenckstern, and M. Grundmann, *Appl. Phys. Lett.* **104**, 022104 (2014).
- [13] H. Mizoguchi, M. Hirano, S. Fujitsu, T. Takeuchi, K. Ueda, and H. Hosono, *Appl. Phys. Lett.* **80**, 1207 (2002).
- [14] D. M. Ramo and P. D. Bristowe, *J. Chem. Phys.* **141**, 084704 (2014).
- [15] T. R. Paudel, A. Zakutayev, S. Lany, M. D'Avezac, and A. Zunger, *Adv. Funct. Mater.* **21**, 4493 (2011).
- [16] K. Nomura, T. Kamiya, and H. Hosono, *Adv. Mater.* **23**, 3431 (2011).
- [17] H. J. Kim, I. C. Song, J. H. Sim, H. Kim, D. Kim, Y. E. Ihm, and W. K. Choo, *J. Appl. Phys.* **95**, 7387 (2004).
- [18] W. Walukiewicz, *Physica B (Amsterdam)* **302**, 123 (2001).
- [19] J. Robertson and S. J. Clark, *Phys. Rev. B* **83**, 075205 (2011).
- [20] J. Robertson, *J. Vac. Sci. Technol. A* **31**, 050821 (2013).
- [21] A. Walsh and K. T. Butler, *Acc. Chem. Res.* **47**, 364 (2014).
- [22] S. Narushima, H. Mizoguchi, K. I. Shimizu, K. Ueda, H. Ohta, M. Hirano, T. Kamiya, and H. Hosono, *Adv. Mater.* **15**, 1409 (2003).
- [23] K. H. L. Zhang, K. Xi, M. G. Blamire, and R. G. Egdell, *J. Phys.: Condens. Matter* **28**, 383002 (2016).
- [24] N. Mansourian-Hadavi, S. Wansom, N. H. Perry, A. R. Nagaraja, T. O. Mason, L.-h. Ye, and A. J. Freeman, *Phys. Rev. B* **81**, 075112 (2010).
- [25] D. O. Scanlon and G. W. Watson, *Phys. Chem. Chem. Phys.* **13**, 9667 (2011).
- [26] K. Samanta, P. Bhattacharya, R. S. Katiyar, W. Iwamoto, R. R. Urbano, P. G. Pagliuso, and C. Rettori, *MRS Proceedings* **891**, 0891-EE10-09 (2005).
- [27] T. Kamiya, S. Narushima, H. Mizoguchi, K. Shimizu, K. Ueda, H. Ohta, M. Hirano, and H. Hosono, *Adv. Funct. Mater.* **15**, 968 (2005).
- [28] M. Dekkers, G. Rijnders, and D. H. A. Blank, *Appl. Phys. Lett.* **90**, 021903 (2007).
- [29] O. Volnianska and P. Boguslawski, *J. Appl. Phys.* **114**, 033711 (2013).
- [30] M. N. Amini, H. Dixit, R. Saniz, D. Lamoen, and B. Partoens, *Phys. Chem. Chem. Phys.* **16**, 2588 (2014).
- [31] G. Kresse and J. Furthmüller, *Phys. Rev. B* **54**, 11169 (1996).
- [32] G. Kresse and J. Furthmüller, *Comput. Mater. Sci.* **6**, 15 (1996).
- [33] G. Kresse and D. Joubert, *Phys. Rev. B* **59**, 1758 (1999).
- [34] J. P. Perdew, A. Ruzsinszky, G. I. Csonka, O. A. Vydrov, G. E. Scuseria, L. A. Constantin, X. Zhou, and K. Burke, *Phys. Rev. Lett.* **100**, 136406 (2008).
- [35] A. Jain, S. P. Ong, G. Hautier, W. Chen, W. D. Richards, S. Dacek, S. Cholia, D. Gunter, D. Skinner, G. Ceder *et al.*, *APL Mater.* **1**, 011002 (2013).
- [36] Materials Project Database item mvc-6068, doi:10.17188/1321879.
- [37] P. E. Blöchl, O. Jepsen, and O. K. Andersen, *Phys. Rev. B* **49**, 16223 (1994).
- [38] J. Kelly and S. G. Alcock, *J. Phys.: Conf. Ser.* **425**, 052024 (2013).

- [39] L. W. Wangoh, S. Sallis, K. M. Wiaderek, Y.-C. Lin, B. Wen, N. F. Quackenbush, N. A. Chernova, J. Guo, L. Ma, T. Wu *et al.*, *Appl. Phys. Lett.* **109**, 053904 (2016).
- [40] N. F. Quackenbush, H. Paik, M. J. Wahila, S. Sallis, M. E. Holtz, X. Huang, A. Ganose, B. J. Morgan, D. O. Scanlon, Y. Gu *et al.*, *Phys. Rev. B* **94**, 085105 (2016).
- [41] K. Fleischer, E. Norton, D. Mullarkey, D. Caffrey, and I. V. Shvets, *Materials* **10**, 1019 (2017).
- [42] J. I. Pankove, *Optical Processes in Semiconductors* (Dover, New York, 1971).
- [43] B. N. Figgis and M. A. Hitchman, *Ligand Field Theory and its Applications*, Special Topics in Inorganic Chemistry (Wiley-VCH, Weinheim, 2000).
- [44] R. Drasovean and S. Condurache-Bota, *J. Optoelectron. Adv. Mater.* **11**, 2141 (2009).
- [45] O. Laporte and W. F. Meggers, *J. Opt. Soc. Am.* **11**, 459 (1925).
- [46] V. F. Drobny and L. Pulfrey, *Thin Solid Films* **61**, 89 (1979).
- [47] E. S. Goh, J. W. Mah, and T. L. Yoon, *Comput. Mater. Sci.* **138**, 111 (2017).
- [48] N. F. Quackenbush, J. P. Allen, D. O. Scanlon, S. Sallis, J. A. Hewlett, A. S. Nandur, B. Chen, K. E. Smith, C. Weiland, D. A. Fischer *et al.*, *Chem. Mater.* **25**, 3114 (2013).
- [49] X. Nie, S.-H. Wei, and S. B. Zhang, *Phys. Rev. Lett.* **88**, 066405 (2002).